RESEARCH PAPER

Synthesize and Characterization of Mesoporous $ZrFe_2O_4@SiO_2$ Core-shell Nanocomposite Modified with APTES and TCPP

*Hamideh Balooch Khosravi, Rahmatollah Rahimi *, Mahboubeh Rabbani *, and Ali Maleki*

Department of Chemistry, Iran University of Science and Technology, Tehran, Iran

ARTICLE INFO

Article History:
Received 11 January 2020
Accepted 02 March 2020
Published 01 April 2020

Keywords:
Core-shell
Mesoporous
Photocatalyst
Porphyrin
Silica
$ZrFe_2O_4$ nanocauliflowers

ABSTRACT

The mesoporous $ZrFe_2O_4$ nanocauliflowers were synthesized via the solvothermal method. The core-shell $ZrFe_2O_4@SiO_2$ nanocomposite was successfully prepared by a simple wet route using tetraethylorthosilicate, then modified with (3-aminopropyl) triethoxisilan (APTES) as linker and tetrakis(4-carboxyphenyl)porphyrin (TCPP) as agent for light harvesting, to fabricate $ZrFe_2O_4@SiO_2$-NH-TCPP nanocomposite. The characterizations of samples were done by Fourier transform infrared spectroscopy (FT-IR), X-ray diffraction (XRD), field emission scanning electron microscopy (FE-SEM), energy dispersive spectroscopy (EDS), nitrogen adsorption and desorption isotherms (BET), vibrating sample magnetometer (VSM), diffuse reflectance spectroscopy (DRS) and fluorescence spectroscopy. The prepared samples were applied as photocatalyst to remove of methyl orange (MO) under visible LED light irradiation. The obtained results showed that the presence of SiO_2 and TCPP decreased the size of particles and improve the photocatalytic activity of samples, too, led to increase of photodegradation of MO. The final fabricated nanocomposite ($ZrFe_2O_4@SiO_2$-NH-TCPP) could degrade MO about 100% under only 10 W visible LED irradiation and be separated easily by an external magnetic field.

How to cite this article
Balooch Khosravi H, Rahimi R, Rabbani M, Maleki A. Synthesize and Characterization of Mesoporous $ZrFe_2O_4@SiO_2$ Core-shell Nanocomposite Modified with APTES and TCPP. J Nanostruct, 2020; 10(2):404-414. DOI: 10.22052/JNS.2020.02.018

INTRODUCTION

Synthetic organic dyes which are widely used in various industries have become a significant source of water pollution. Methyl orange (MO) is a dye, which used in many industries, having various harmful effects on humans when released into the environment [1,2]. Therefore, removal of this dye from wastewater has been extensively studied [1,3].

In the past decade, magnetic nanoparticles have been considered to surface functionalization, such as a coating which could result in obtaining significant properties such as photocatalytic activity [4]. Although there are many kinds of materials available for coatings of the magnetic nanoparticles, such as metal oxide, noble metals and polymer materials, the silica is still considered to be the best candidate for surface functionalization because it is highly stable against degradation [5].

In the literature, there are only few studies on Zr-substituted magnetite [6-12]. To knowledge, the structural and magnetic properties of $ZrFe_2O_4$, models of the distribution of Fe^{2+}, Fe^{3+} and Ti^{4+} ions in $TiFe_2O_4$ have been used because Zr is one of the family group of Ti [6,7,9-14].

There are several methods to prepare of ferrites, such as microwave [15], solvothermal [16], mechanochemical [17], sonochemical [18] and wet chemical methods [19]. It seems that a one-pot template-free solvothermal method in ethylene glycol (EG) as solvent and ammonium acetate as electrostatic stabilization to be the preferred method [16,20].

On ther other hands, covering the surface of ferrites nanoparticles by the silica shell, not only protected the magnetic cores against aggregating, but also made it easy to introduce new functional

* *Corresponding Author Email: rahimi_rah@iust.ac.ir*

groups. To achive this gole, tetraethylorthosilicate (TEOS) is a proper material. It can be hydrolyzed to silica by ammonia (pH=10-12), which makes it an excellent system for uniform coating on nanomagnetic particles. [21].

Foretheremore, porphyrins are known as attractive compounds in chemical science because of its heterocyclic building blocks with a highly π-conjugated system They have considerable catalytic properties due to their interesting chemical and photochemical characteristics. The meso position of the porphyrin is one of the most reactive centers; the substituent effect on the electrochemical property of porphyrins that influence the efficiency of catalytic and electron transfer processes [22,23]. TCPP (5,10,15,20-meso-tetrakis(4-carboxyphenyl)porphyrin) is a kind of porphyrin, consists of a porphin ring and four benzoic acid groups. These macromolecules can be linked to magnetic materials [24], which can influence the electron transfer of porphyrins [25-30].

In this study, mesoporous $ZrFe_2O_4$ nanocauliflowers were synthesized as the core, then were coated by SiO_2 as the shell, finally modified by TCPP. The prepared nanocomposite was applied as an environmentally friendly photocatalyst to remove of methyl orange (MO) under visible LED lamp light.

MATERIALS AND METHODS

Chemicals

In this study, zirconium chloride ($ZrCl_4$), iron (III) chloride ($FeCl_3.6H_2O$), ethylene glycol ($C_2H_6O_2$), ammonium acetate (NH_4.OAC), ethanol (C_2H_5OH) 96% and 99%, tetraethylorthosilicate (TEOS), dry toluene (C_7H_8), (3-aminopropyl)triethoxisilan (APTES) and all the chemicals, solvents and reagents were purchased from Aldrich and Merck have been used without any further purification.

Synthesis of mesoporous $ZrFe_2O_4$ nanocauliflowers

First, 1 mmol (0.233 g) $ZrCl_4$ and 2 mmol (0.541 g) $FeCl_3.6H_2O$ were dissolved in 50 mL ethyleneglycol at vigorously stirred at 600 rpm for15 min to form a clear solution. Then 30 mmol (1.156 g) NH_4.OAC as a protective agent, was added into the mixture solution under an ultrasonic bath for 30 min to form a dark yellow solution. In continuing, the condition in vigorously stirred at 600 rpm for 30 min at room temperature. Afterward, the mixture was sunk in a 50 mL Teflon-line stainless steel autoclave, fixed and kept in at 210 °C for 48 h. As a result, the black precipitate was collected by an extrnal magnetic field and washed with ethanol and distilled water several times. At last, products were dried in a vacuum system at 60 °C for 15 h [15].

Synthesis of $ZrFe_2O_4@SiO_2$-NH_2

$ZrFe_2O_4@SiO_2$ nanocomposite was obtained by the Stober method [15]. To synthesis of $ZrFe_2O_4@SiO_2$-NH_2, 0.5 g (1.54 mmol) $ZrFe_2O_4@SiO_2$ was dispersed in 10 mL dry toluene and 0.5 mL (2.5 mmol) APTES was added under N_2 atmosphere. Subsequently, the mixture was refluxed for 18 h. The obtained product was washed by hot toluene and dried in a vacuum oven [31].

Synthesis of $ZrFe_2O_4@SiO_2$-NH-TCPP

Synthesis of $ZrFe_2O_4@SiO_2$-NH-TCCP was carried out by mixing and $ZrFe_2O_4@SiO_2$-NH_2 nanocomposite in the ratio of 1:20. Therefore, 0.01 g TCCP and 0.2 g $ZrFe_2O_4@SiO_2$-NH_2 were added to 150 mL DMF and refluxed for 8 hour by a magnetic stirrer. The obtained product was washed with distilled water and dried in a vacuum oven [32].

Equipment and characterization

The functional groups of the materials were recorded by Fourier transform infrared spectroscopy (FT-IR) on a Shimadzu FTIR 8400S spectrophotometer with KBr pellet. X-ray diffraction (XRD) analysis was performed on Philips Pw 1730 X-ray diffractometer with Cu Kα radiation. The morphology of the synthesized samples was observed by a Tescan Mira3 field emission scanning electron microscopy (FE-SEM). The elemental constituents of samples were obtained by energy-dispersive X-ray spectroscopy (EDS) using VEGAII, Tescan, Czech Republic instruments. The nitrogen (N_2) adsorption and desorption equipment, Brunauer-Emmett-Teller (BET) surface areas and Barrett-Joyner-Halenda (BJH) pore sizes were calculated on an ASAP 2020 (Micromeritics Ins. Corp.) at liquid nitrogen. Also vibrating sample magnetometer (VSM, MDKB, Magnetic Daghigh Kavir Co. Iran) was employed to measure the magnetic behavior of nanomagnetic particles at room temperature. Shimadzu (UV-2550) spectrophotometer obtained the diffuse reflectance spectroscopy (DRS) spectra. Spectrofluorophotometer (RF-6000, Shimadzu)

was used to characterize the optical properties of material.

Photocatalytic experiments under visible light irradiation

The photocatalytic activity of the prepared samples was evaluated by degradation of MO solutions. In a typical process, the catalytic reaction was carried out in a 100 mL photoreactor, which contains 50 mL of MO dye solutions with a concentration of 10 mg L^{-1} (pH=3) and 5 mg of catalyst. Irradiation was provided using a 10 W LED lamps as the light sources for one hour. All photocatalytic tests were carried out at the same conditions. The concentration of MO dye was monitored using a UV-Vis spectrophotometer (Shimadzu UV-1700) at 464 nm.

RESULTS AND DISCUSSION

FT-IR spectra of the prepared samples

FT-IR spectra of $ZrFe_2O_4$, $ZrFe_2O_4@SiO_2$, $ZrFe_2O_4@SiO_2$-TCPP, and $ZrFe_2O_4@SiO_2$-NH-TCPP are shown in Fig. 1. Peaks at 585 and 455 cm^{-1} belong to Fe-O and Zr-O bands, respectively. The peaks at 3444, 1645 and 1398 cm^{-1} point out the presence of O-H stretching bending and deforming vibration of adsorbed water [33]. At spectrum of $ZrFe_2O_4@SiO_2$, the new sharp peaks at 1090, 800 and 470 cm^{-1} are assigned to the asymmetry stretching, symmetric stretching and bending vibrations of Si-O of the silica shell on the $ZrFe_2O_4$ nanocauliflowers, respectively [21].

The $ZrFe_2O_4@SiO_2$-NH_2 spectrum, the broad peak around 3400 cm^{-1} corresponds to N-H stretching modes, and the peak at 1060 cm^{-1} indicate the existence of a terminal $–NH_2$ of APTES, however, this peak has been protected by stretching vibration of Si-O of silica. The peaks that appeared at 835 cm^{-1} could be assigned to the bending vibrant of C-H from APTES [21].

In spectra of $ZrFe_2O_4@SiO_2$-TCPP and $ZrFe_2O_4@SiO_2$-NH-TCPP, the presence of the peak at 3200

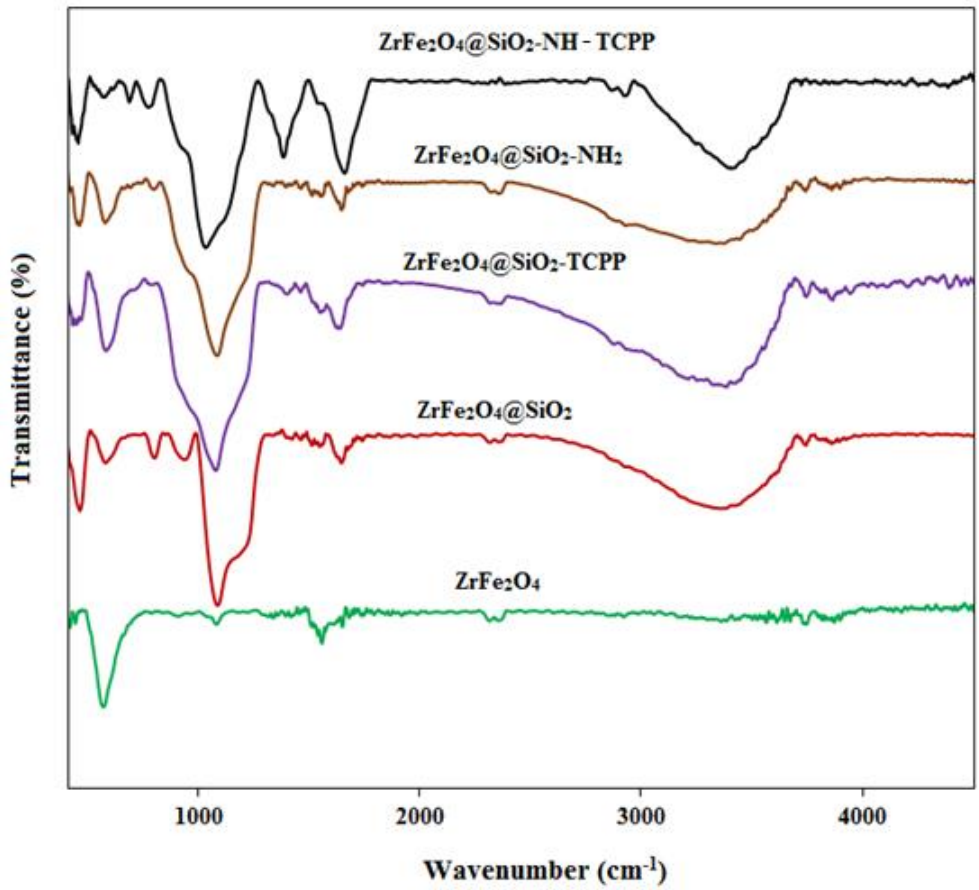

Fig. 1. The FT-IR spectra of the prepared samples.

cm^{-1} approve N-H bending vibration band of pyrrole ring, and at 2900 cm^{-1} show the C-H stretching vibration of aryl group which corresponds to TCPP. Referring to the FT-IR spectrum of pure TCPP, a sharp C=O stretching peak can be observed at approximately 1700 cm^{-1} [34].

Structural characterization of the prepared samples

Fig. 2 shows the XRD patterns of $ZrFe_2O_4$, $ZrFe_2O_4@SiO_2$, $ZrFe_2O_4@SiO_2$-TCPP and $ZrFe_2O_4@SiO_2$-NH-TCPP. It confirms that all the samples were formed in an inverse spinel structure similar to that of magnetite (space group Fd3m, No. 227, with standard card JCPDS No. 01-088-0315). According to the Debye–Scherrer formula, the crystalline size of the sample is given by:

$$D=0.9\lambda/\beta\cos\theta \quad (1)$$

Where β is the full-width at half-maximum (FWHM) value of XRD diffraction lines, the wavelength λ = 0.154056 nm and θ is the half diffraction angle of 2θ. The size of crystalline of $ZrFe_2O_4$ nanocauliflowers was found 44.6 mm, which calculated by taking the average of the sizes at its peaks. The intensity of the peaks decreased after immobilizing of silica on the surface of ferrite particles. In this pattern, no extra peaks for other phases were detected, and no redundant reaction had occurred between the core and shell.

The crystallite size of $ZrFe_2O_4$, $ZrFe_2O_4@SiO_2$, $ZrFe_2O_4@SiO_2$-TCPP and $ZrFe_2O_4@SiO_2$-NH-TCPP based on Scherrer equation was 41.3, 36.9, 34.8 and 26.5 respectively, indicated that after coating of ferrite with SiO_2 and modifying by APTES and TCPP, the crystallite size of nanostructures has been decreased.

Morphological characterization of the prepared samples

The microstructure of the samples can be identified by scanning electron microscope (SEM) tool. Fig. 3 shows the morphology of high resolution and nanosize is the most regular shape of the particle. $ZrFe_2O_4$ particles with an average size of 35 nm were agglomerated to form nanocauliflowers with an average size of 150 nm. Ethylene glycol and ammonium acetate play essential roles in the self-assembly of the nanocrystals and fabrication of monodisperse fine metal oxides (Fig. 4). SEM images of prepared nanocomposites indicate that after SiO_2 coating and functionalizing (with APTES, and TCPP), the

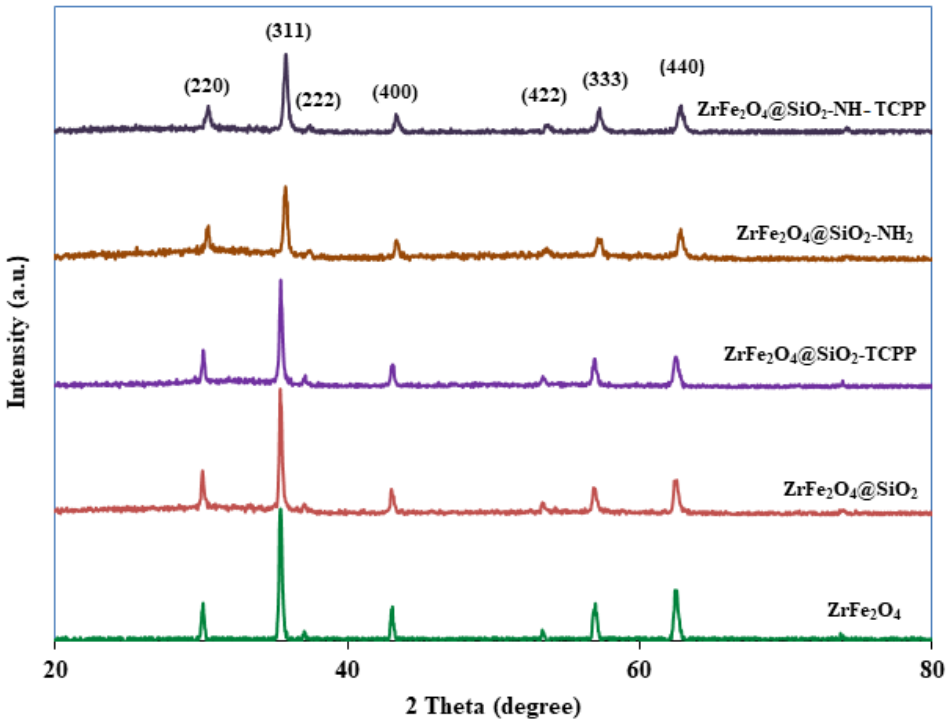

Fig. 2. The XRD pattern of the prepared samples.

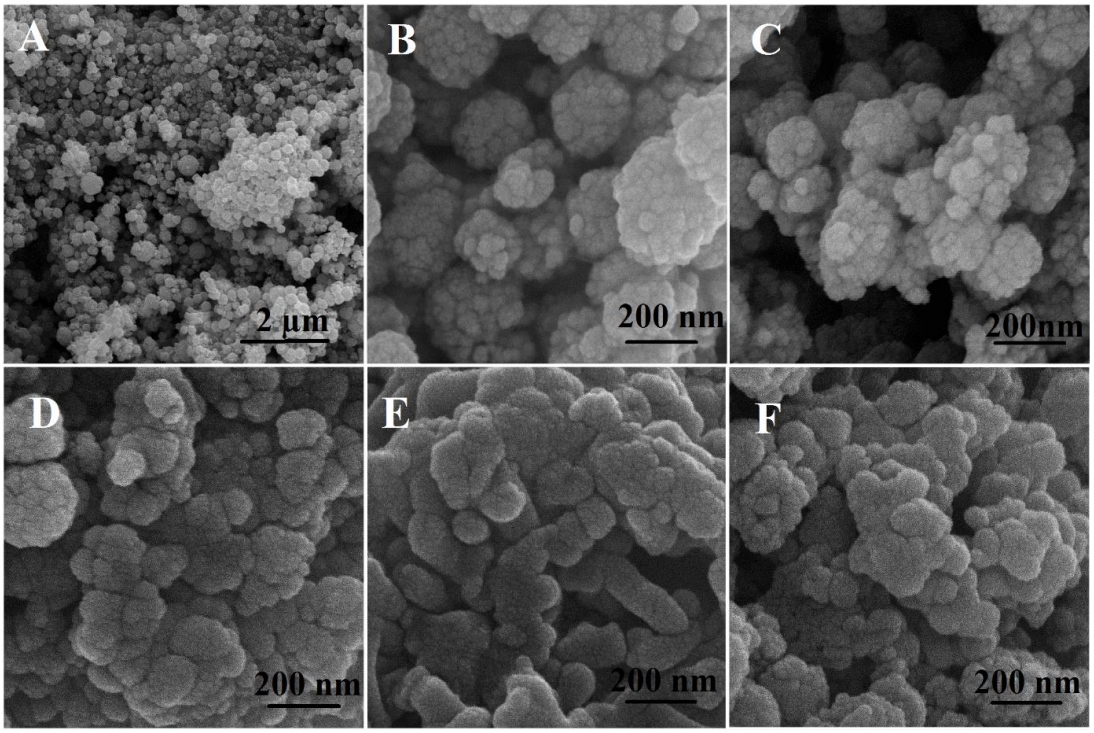

Fig. 3. The SEM images of (A,B) $ZrFe_2O_4$, (C) $ZrFe_2O_4@SiO_2$, (D) $ZrFe_2O_4@SiO_2$-NH_2, (E) $ZrFe_2O_4@SiO_2$-TCPP and (F) $ZrFe_2O_4@SiO_2$-NH-TCPP.

average size of nanoparticles decreased to 32, 29, 25, and 23 nm for $ZrFe_2O_4$, $ZrFe_2O_4@SiO_2$, $ZrFe_2O_4@SiO_2$-TCPP, and $ZrFe_2O_4@SiO_2$-NH-TCPP, respectively.

Fig. 5 shows the typical TEM images of the $ZrFe_2O_4@SiO_2$-NH-TCPP nanocomposite, which indicates a well-defined core-shell mesoporous nanostructure. The amount of thickness the shell layer, containing silica and porphyrin is about 10-9 nm.

Elemental analysis of $ZrFe_2O_4$ and $ZrFe_2O_4@SiO_2$

To identify the elemental composition of mesoporous $ZrFe_2O_4$ nanocauliflowers and $ZrFe_2O_4@SiO_2$, an energy-dispersive X-ray spectroscopy (EDS) was used. As can be seen in Fig. 6, EDS pattern of $ZrFe_2O_4$ nanocauliflowers shows the peaks of Fe, Zr, Si and O elements, and approves

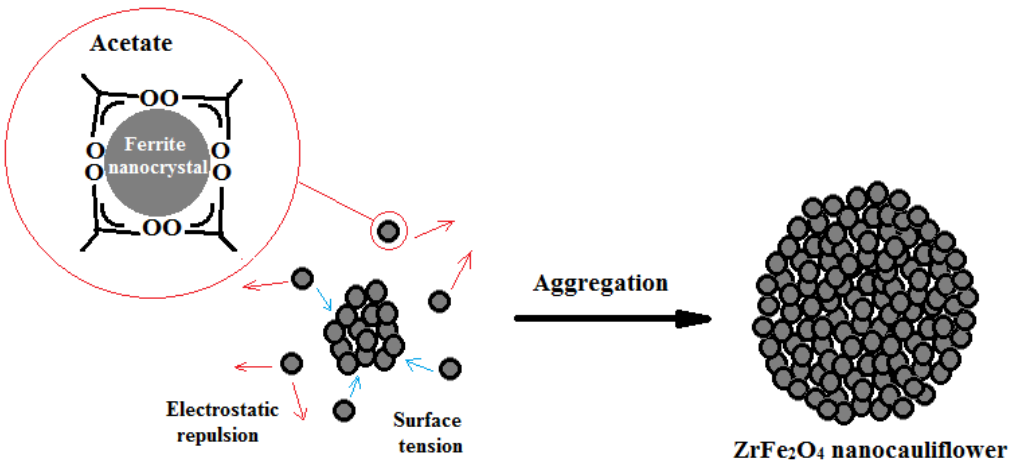

Fig. 4. Proposed mechanism for the formation of mesoporous Zr ferrite particles.

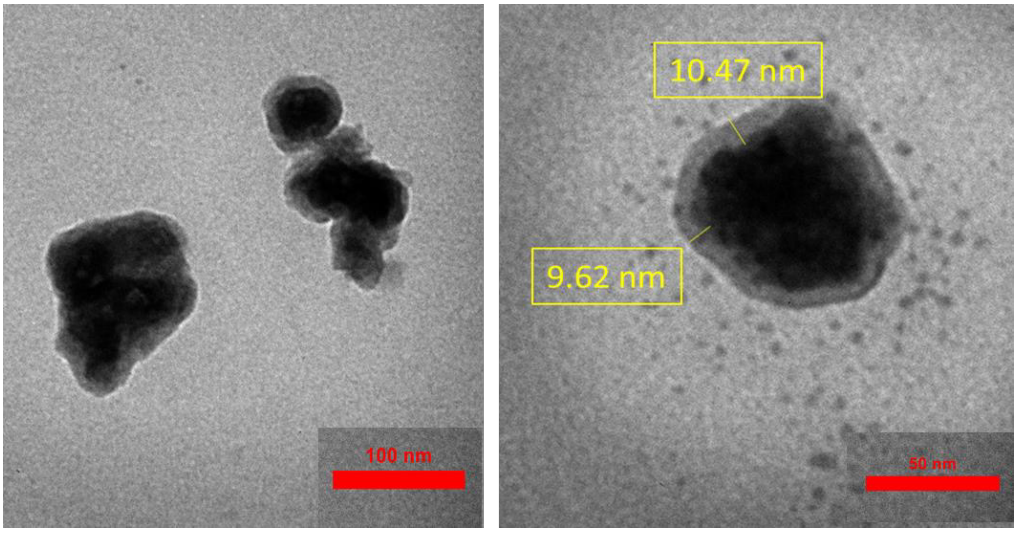

Fig. 5. The TEM images of $ZrFe_2O_4$@SiO_2-NH-TCPP.

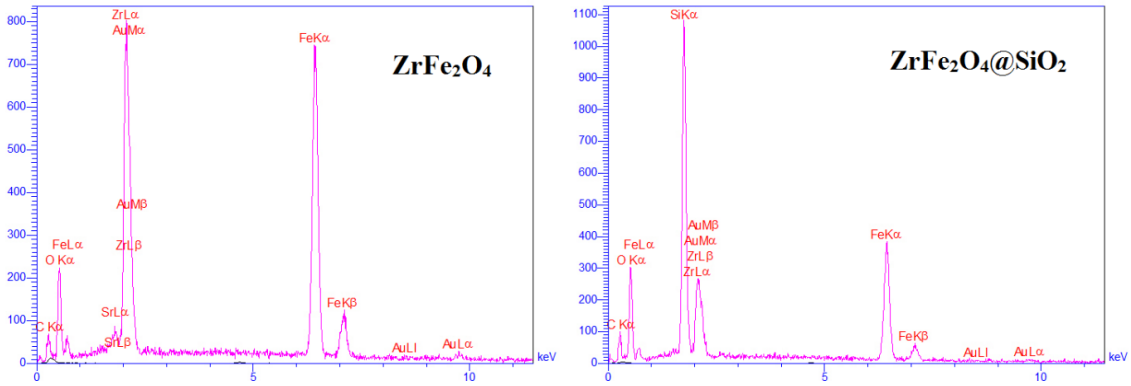

Fig. 6. The EDS analysis of $ZrFe_2O_4$ and $ZrFe_2O_4$@SiO_2.

the presence of the iron and zirconium elements in the molar ratio of 2:1. Chemical characterization of the $ZrFe_2O_4$@SiO_2 sample showed that it was composed of iron, zirconium, oxygen and silicon elements, provide the existence of SiO_2 on surface of $ZrFe_2O_4$. Furthermore, the molar ratio of SiO_2 to $ZrFe_2O_4$ was 10:1, which confirmed by XRF analysis of samples.

Nitrogen adsorption and desorption isotherms of $ZrFe_2O_4$ and $ZrFe_2O_4$@SiO_2-NH-MnTCPP

The specific surface area and pore volume data of the mesoporous $ZrFe_2O_4$ nanocauliflowers and $ZrFe_2O_4$@SiO_2-NH-TCPP composite were characterized using the N_2 adsorption-desorption method, with a typical isotherm shown in Fig. 7. The isotherm demonstrates a type IV isotherm. Data obtained by BET also showed large surface areas for the $ZrFe_2O_4$ and $ZrFe_2O_4$@SiO_2-NH-TCPP composite (431 and 978 m^2g^{-1}, respectively). These values are relatively large compared to other reported mesoporous ferrite structures [35]. The very uniform pore sizes of the $ZrFe_2O_4$ and $ZrFe_2O_4$@SiO_2-NH-TCPP were found to be 5.8635, and 4.5345 nm, respectively. The decreasing particle size of composite rather than pure ferrite can lead to the decrease of pore size and increase of surface area and pore volume of the nanocomposite. The pore volume of $ZrFe_2O_4$ and $ZrFe_2O_4$@SiO_2-NH-TCPP composite was calculated 0.5812 and 0.9692 cm^3/g, respectively. The $ZrFe_2O_4$@SiO_2-NH-TCPP composite showed higher textural mesoporosity, volume that facilitates the achievement in its area of the scaffold-

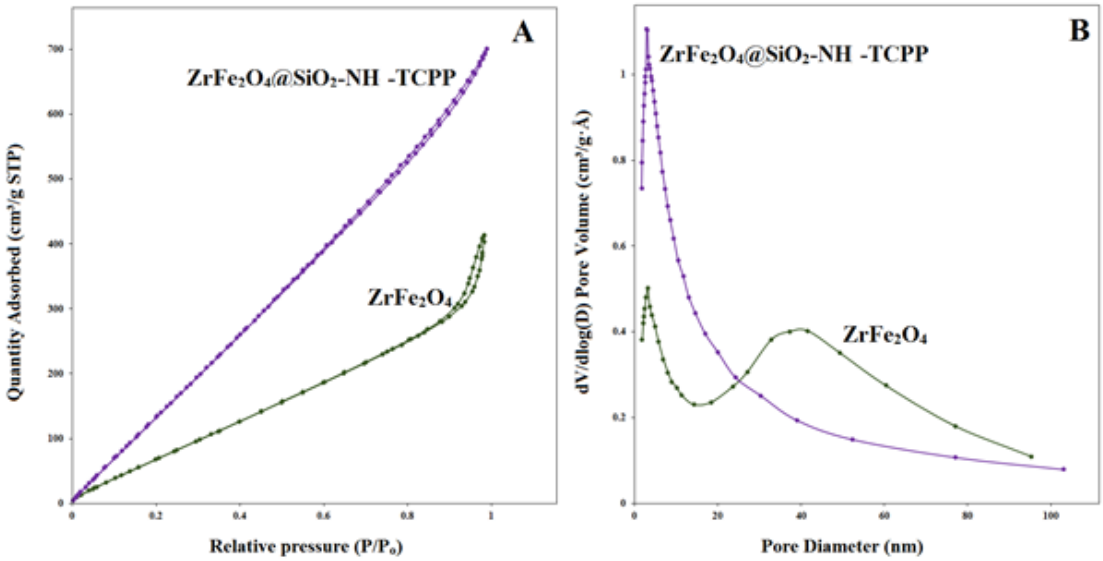

Fig. 7. (A) N_2 adsorption–desorption isotherms and (B) pore size distributions from the desorption branches through the BJH method of $ZrFe_2O_4$ and $ZrFe_2O_4@SiO_2$-NH-TCPP.

confined mesoporosity, and modifying its catalytic properties.

Magnetic properties of the prepared samples

The magnetic properties of mesoporous $ZrFe_2O_4$ nanocauliflowers were measured at room temperature by using VSM in an external magnetic field ranging from -8 kOe to 8 kOe and compared with the coated material (SiO_2 and TCPP) as the shell which is synthesized, $ZrFe_2O_4@SiO_2$, $ZrFe_2O_4@SiO_2$-TCPP and $ZrFe_2O_4@SiO_2$-NH-TCPP (Fig. 8).

The saturation magnetization (Ms) value, extracted from the corresponding hysteresis loop, from the uncoated ferrite sample at 300 K, is 18.3 emu/g. Ms decreased for the coated samples as expected to be 12.4, 5.7, 4.1 and 2.8 emu/g for $ZrFe_2O_4$, $ZrFe_2O_4@SiO_2$, $ZrFe_2O_4@SiO_2$-TCPP and $ZrFe_2O_4@SiO_2$-NH-TCPP, respectively, demonstrates that SiO_2 and TCPP have been successfully immobilized on the surface of $ZrFe_2O_4$ nanocauliflowers. By coating the silica on ferrite, the Fe ions tend to bond with silica (Fe-O-Si), so the magnetic moment of Fe ions would get diminished [36]. The same reason, the presence of TCPP causes for a decrease in the magnetic properties of the nanomagnetic particles. However their magnetic properties are still significant for the separation of these particles (as a catalyst) by using an external magnetic field.

The coercivity (Hc) values are little increased in the range of 50 Oe for the bare magnetite nanocauliflowers to 100, 100, 150 and 150 Oe for $ZrFe_2O_4@SiO_2$, $ZrFe_2O_4@SiO_2$-NH-TCPP and $ZrFe_2O_4@SiO_2$-TCPP, respectively. This increasing can be occurred due to the shrinking of ferrite nanoparticles after immobilizing of SiO_2 and functionalizing with TCPP. In a single-domain particle, all the spins are aligned in the same direction, and the particle is uniformly magnetized. Because there are no domain walls to move, the magnetization will be reversed through spin rotation rather than through the motion of domain walls, leads to large coercivity of the nanoparticles [37]. Another possible explanation for this result could be as follows: The magnetic moments of magnetic nanoparticles are pined by the SiO_2 and TCPP, so that a higher magnetic field is required to align the single domain nanoparticles in the field direction [34].

Optical properties of the prepares samples

The optical properties of the synthesized materials were studied by the UV–Vis diffuse reflectance spectrophotometer (DRS). The obtained curves are shown in Fig. 9A. $ZrFe_2O_4@SiO_2$ exhibited slightly weaker absorption in the range of 200–800 nm than $ZrFe_2O_4$ nanocauliflowers, probably resulting from the light reflection and refraction of SiO_2 [38]. In the $ZrFe_2O_4@SiO_2$-NH-TCPP spectrum, the peak observed at 440 nm can be corresponded to the soret band of porphyrin

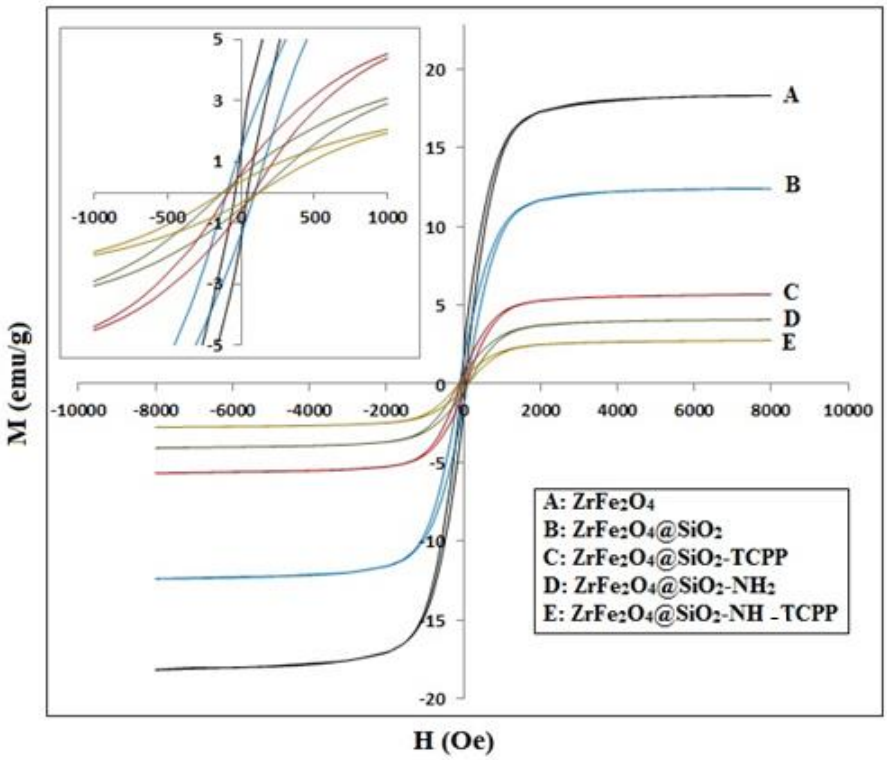

Fig. 8. The magnetization curves of the prepared samples.

that confirms immobilizing of porphyrin on the surface of $ZrFe_2O_4@SiO_2$ nanocomposite. It can be seen that a red shift in $ZrFe_2O_4@SiO_2$-NH-TCPP nanocomposites was obtained in comparison with pure porphyrin. This means that the $ZrFe_2O_4@SiO_2$-NH-TCPP nanocomposite is sensitive to visible light, which accounts for the photoactivity under visible light irradiation. It is generally accepted that the red shift of the absorption band can increase photon numbers by extending the energy range of photoexcitation, which can be absorbed by the catalyst and utilized for the photocatalytic reaction.

The bandgap energy can be approximately calculated from 1.4-1.7 eV (Fig. 9B). The results of the experiments confirm that modifying the

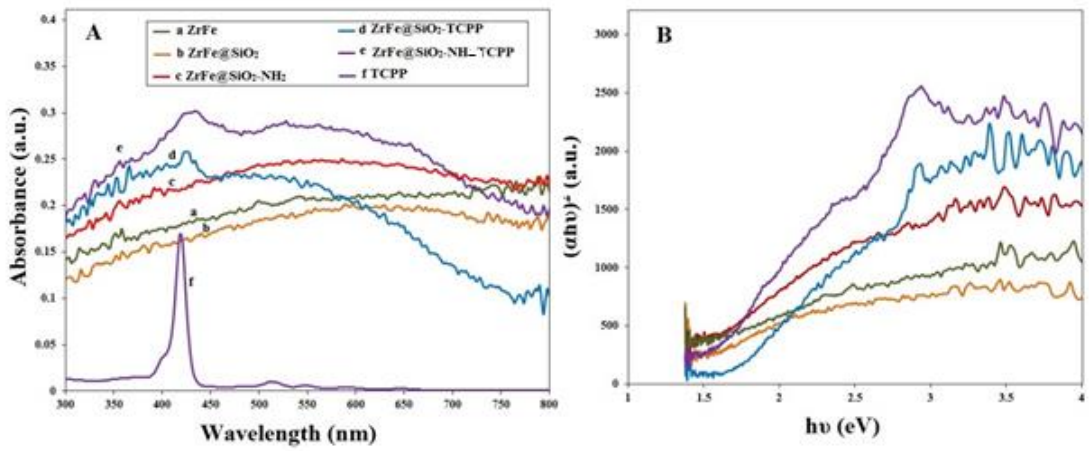

Fig. 9. (A) The DRS and (B) the band gap of the prepared samples.

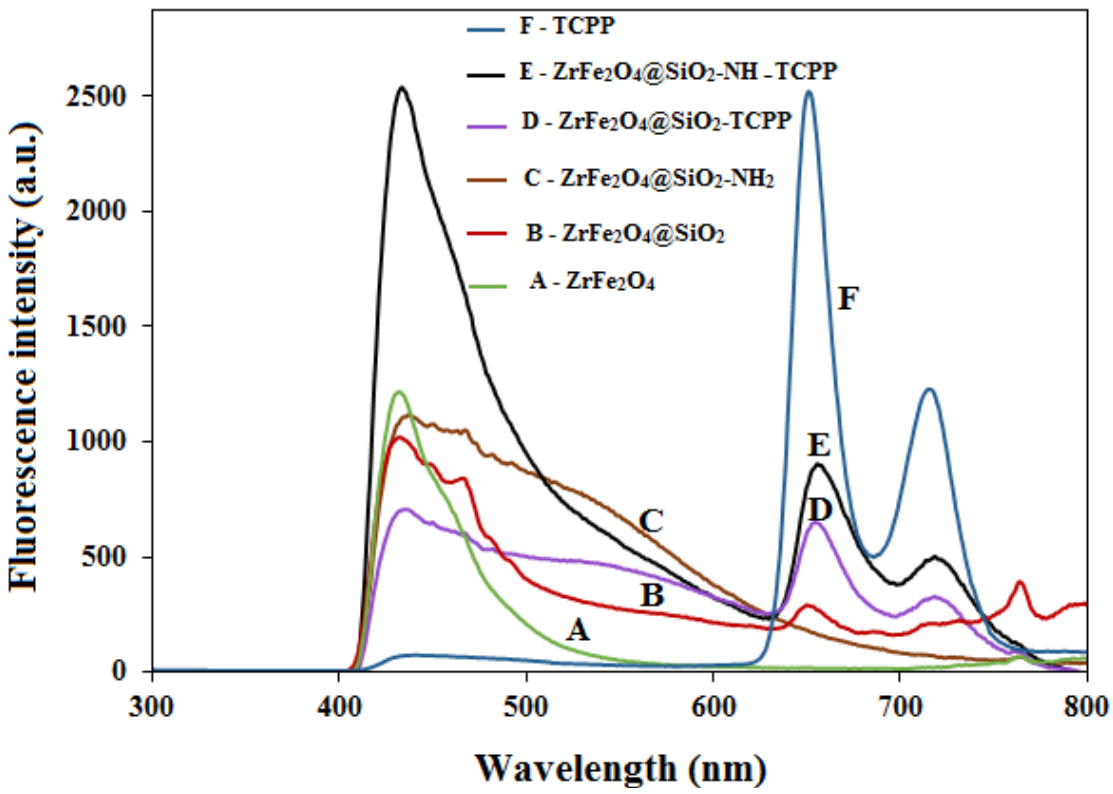

Fig. 10. The fluorescence of the prepared samples.

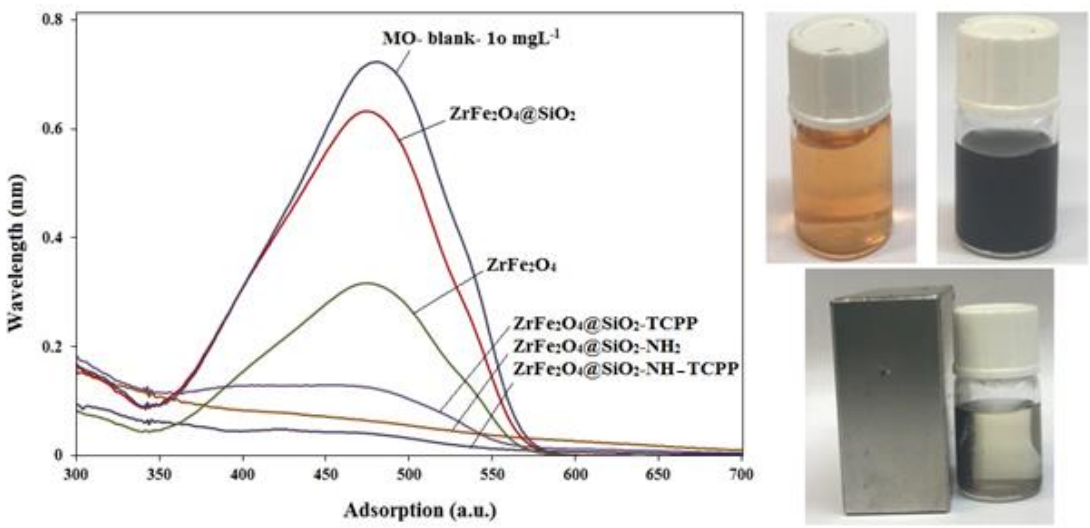

Fig. 11. The photocatalytic degradation process of MO (initial concentration: 10 mgL^{-1}, 50 mL) using 0.05 g of the prepared samplers after 1 h irradiation by LED light.

surface of the composite with porphyrin play a crucial role in enhancing the photocatalytic performance of $ZrFe_2O_4@SiO_2$ nanocomposite for MO degradation.

Fluorescence spectra of the prepared samples

The fluorescence spectra of the prepared samples, shown in Fig. 10, give more detailed information. The emission spectra of the all

prepared samples have shown emission peak at 430 nm (excitation peaks at 400 nm), but TCPP has illustrated two peaks at 663 and 733 nm with significant quenching after immunizing on the surface of nanocomposite ($ZrFe_2O_4@SiO_2$-TCPP, and $ZrFe_2O_4@SiO_2$-NH-TCPP) when compared to the original porphyrin. Such quenching of emissions is predicted that can be attributed to the binding of the porphyrin to the nanocomposite surface and transferring photogenerated electrons of TCPP on nanocomposite.

Photocatalytic activity of the prepared samples

The photocatalytic activity of the prepared samples was investigated by performing experiments on the degradation of 10 mg L^{-1} methyl orange. The photodegradation results were shown in Fig. 11. As can be seen from this figure, the excellent catalytic activity of photocatalysts with mesoporous structure is assigned to the mesoporous network structure. The higher surface area in $ZrFe_2O_4@SiO_2$-NH-TCPP is beneficial to raise the number of active sites of these photocatalysts, so exhibited the highest activity to degrade methyl orange.

CONCLUSION

In this work, core–shell structured $ZrFe_2O_4@SiO_2$ nanocauliflowers were fabricated and modified with 3-aminopropyltriethoxysilane as a linker, and tetrakis(4-carboxyphenyl)porphyrin as a sensitizer agent. Based on the XRD, FT-IR, SEM, TEM, EDS, BET, VSM, DRS and fluorescence analysis results, as-prepared nanocomposite can be extended to synthesize mesoporous texture magnetic nanocomposites with large specific surface areas and narrow size distribution. Study on photocatalytic activity of the prepared samples for removal of methyl orange from aqua solutions showed that the final fabricated nanocomposite ($ZrFe_2O_4@SiO_2$-NH-TCPP) could degrade this pollutant about 100% under only 10 W LED lamp irradiation. The obtaine results indicated that the synthesized nanocomposite not only shows excellent photocatalytic activity for removal of MO, but also can be separated easily by an external magnetic field.

CONFLICT OF INTEREST

The authors declare that there is no conflict of interests regarding the publication of this paper.

REFERENCES

1. Rahimi R, Kharazi P, Rabbani M. Synthesis and characterization of magnetically separable visible-light photocatalyst for removal of methyl orange. Proceedings of The 21st International Electronic Conference on Synthetic Organic Chemistry; 2017/11/03: MDPI; 2017.
2. Zhang Y, Nan Z. Preparation of magnetic $ZnLa_{0.02}Fe_{1.98}O_4$/MWCNTs composites and investigation on its adsorption of methyl orange from aqueous solution. Mater Res Bull. 2015;66:176-185.
3. Rameshbabu R, Kumar N, Karthigeyan A, Neppolian B. Visible light photocatalytic activities of $ZnFe_2O_4$ /ZnO nanoparticles for the degradation of organic pollutants. Mater Chem Phys. 2016;181:106-115.
4. Su M, He C, Sharma VK, Abou Asi M, Xia D, Li X-z, et al. Mesoporous zinc ferrite: Synthesis, characterization, and photocatalytic activity with H_2O_2/visible light. J Hazard Mater. 2012;211-212:95-103.
5. Dupont D, Luyten J, Bloemen M, Verbiest T, Binnemans K. Acid-Stable Magnetic Core–Shell Nanoparticles for the Separation of Rare Earths. Ind Eng Chem Res. 2014;53(39):15222-15229.
6. Bosi F, Halenius U, Skogby H. Crystal chemistry of the magnetite-ulvospinel series. Am Mineral. 2009;94(1):181-189.
7. O'Reilly W, Banerjee SK. Cation distribution in titanomagnetites $(1-x)Fe_3O_{4-x}Fe_2TiO_4$. Phys Lett. 1965;17(3):237-238.
8. Akimoto S-i, Katsura T, Yoshida M. Magnetic Properties of $TiFe_2O_4$-Fe_3O_4 System and Their Change with Oxidation. Journal of geomagnetism and geoelectricity. 1957;9(4):165-178.
9. Sorescu M, Xu T, Wise A, Díaz-Michelena M, McHenry ME. Studies on Structural, Magnetic and Thermal Properties of $xFe_2TiO_{4-(1-x)}Fe_3O_4$ ($0 \le x \le 1$) Pseudo-binary System. J Magn Magn Mater. 2012;324(7):1453-1462.
10. Moskowitz BM, Jackson M, Kissel C. Low-temperature magnetic behavior of titanomagnetites. Earth Planet Sci Lett. 1998;157(3-4):141-149.
11. Hamdeh HH, Barghout K, Ho JC, Shand PM, Miller LL. A Mössbauer evaluation of cation distribution in titanomagnetites. J Magn Magn Mater. 1999;191(1-2):72-78.
12. Sattar AA, El-Sayed HM, Agami WR, Ghani AA. Magnetic Properties and Electrical Resistivity of Zr^{4+} Substituted Li-Zn Ferrite. American Journal of Applied Sciences. 2007;4(2):89-93.
13. Gurav SK, Shirsath SE, Kadam RH, Patange SM, Lohar KS, Mane DR. Less magnetic and larger Zr^{4+}–Zn^{2+} ions co-substituted structural and magnetic properties of ordered $Li_{0.5}Fe_{2.5}O_4$ nanoparticles. Mater Res Bull. 2013;48(9):3530-3536.
14. Das AR, Ananthan VS, Khan DC. Lattice parameter variation and magnetization studies on titanium-, zirconium-, and tin-substituted nickel-zinc ferrites. J Appl Phys. 1985;57(8):4189-4191.
15. Rezaei A, Nabiyouni G, Ghanbari D. Photo-catalyst and magnetic investigation of $BaFe_{12}O_{19}$–ZnO nanoparticles and nanocomposites. Journal of Materials Science: Materials in Electronics. 2016;27(11):11339-11352.
16. Rahimi R, Kerdari H, Rabbani M, Shafiee M. Synthesis, characterization and adsorbing properties of hollow Zn-

Fe_2O_4 nanospheres on removal of Congo red from aqueous solution. Desalination. 2011;280(1-3):412-418.
17. Rabbani M, Rafiee F, Ghafuri H, Rahimi R. Synthesis of Fe_3O_4 nonoparticles via a fast and facile mechanochemicl method: Modification of surface with porphyrin and photocatalytic study. Mater Lett. 2016;166:247-250.
18. Jiang W, Zhang X, Gong X, Yan F, Zhang Z. Sonochemical synthesis and characterization of magnetic separable Fe_3O_4–TiO_2 nanocomposites and their catalytic properties. International Journal of Smart and Nano Materials. 2010;1(4):278-287.
19. Wu W, Xiao X, Zhang S, Ren F, Jiang C. Facile method to synthesize magnetic iron oxides/TiO2 hybrid nanoparticles and their photodegradation application of methylene blue. Nanoscale Research Letters. 2011;6(1):533.
20. Wan J, Cai W, Meng X, Liu E. Monodisperse water-soluble magnetite nanoparticles prepared by polyol process for high-performance magnetic resonance imaging. Chem Commun. 2007(47):5004.
21. Maleki A, Kari T, Aghaei M. $Fe_3O_4@SiO_2@TiO_2$-OSO_3H: an efficient hierarchical nanocatalyst for the organic quinazolines syntheses. J Porous Mater. 2017;24(6):1481-1496.
22. Groves JT, Shalyaev K, Lee J. Oxometalloporphyrins in Oxidative Catalysis. ChemInform. 2003;34(19).
23. Stephenson NA, Bell AT. Effects of porphyrin composition on the activity and selectivity of the iron(III) porphyrin catalysts for the epoxidation of cyclooctene by hydrogen peroxide. J Mol Catal A: Chem. 2007;272(1-2):108-117.
24. Laybourn A, Dawson R, Clowes R, Hasell T, Cooper AI, Khimyak YZ, et al. Network formation mechanisms in conjugated microporous polymers. Polym Chem. 2014;5(21):6325-6333.
25. Monnereau C, Gomez J, Blart E, Odobel F, Wallin S, Fallberg A, et al. Photoinduced Electron Transfer in Platinum(II) Terpyridinyl Acetylide Complexes Connected to a Porphyrin Unit. Inorg Chem. 2005;44(13):4806-4817.
26. Kira A, Umeyama T, Matano Y, Yoshida K, Isoda S, Park JK, et al. Supramolecular Donor−Acceptor Heterojunctions by Vectorial Stepwise Assembly of Porphyrins and Coordination-Bonded Fullerene Arrays for Photocurrent Generation. J Am Chem Soc. 2009;131(9):3198-3200.
27. Liu C-y, Bard AJ. Optoelectronic Properties and Memories Based on Organic Single-Crystal Thin Films. Acc Chem Res. 1999;32(3):235-245.
28. Fungo F, Otero L, Borsarelli CD, Durantini EN, Silber JJ, Sereno L. Photocurrent Generation in Thin SnO2Nanocrystalline Semiconductor Film Electrodes from Photoinduced Charge-Separation State in Porphyrin−C60Dyad. The Journal of Physical Chemistry B. 2002;106(16):4070-4078.
29. Gervaldo M, Fungo F, Durantini EN, Silber JJ, Sereno L, Otero L. Carboxyphenyl Metalloporphyrins as Photosensitizers of Semiconductor Film Electrodes. A Study of the Effect of Different Central Metals. The Journal of Physical Chemistry B. 2005;109(44):20953-20962.
30. Drain CM, Varotto A, Radivojevic I. Self-Organized Porphyrinic Materials. Chem Rev. 2009;109(5):1630-1658.
31. Liu F, Niu F, Peng N, Su Y, Yang Y. Synthesis, characterization, and application of $Fe_3O_4@SiO_2$–NH_2 nanoparticles. RSC Advances. 2015;5(23):18128-18136.
32. Li D, Dong W, Sun S, Shi Z, Feng S. Photocatalytic Degradation of Acid Chrome Blue K with Porphyrin-Sensitized TiO_2 under Visible Light. The Journal of Physical Chemistry C. 2008;112(38):14878-14882.
33. Gangwar A, Alla SK, Srivastava M, Meena SS, Prasadrao EV, Mandal RK, et al. Structural and magnetic characterization of Zr-substituted magnetite ($Zr_xFe_{3-x}O_4$, $0 \le x \le 1$). J Magn Magn Mater. 2016;401:559-566.
34. Rahimi R, Zargari S, Yousefi A, Yaghoubi Berijani M, Ghaffarinejad A, Morsali A. Visible light photocatalytic disinfection of E. coli with TiO_2 –graphene nanocomposite sensitized with tetrakis(4-carboxyphenyl)porphyrin. Appl Surf Sci. 2015;355:1098-1106.
35. Wang Y, Zhao H, Li M, Fan J, Zhao G. Magnetic ordered mesoporous copper ferrite as a heterogeneous Fenton catalyst for the degradation of imidacloprid. Applied Catalysis B: Environmental. 2014;147:534-545.
36. Abbas M. Fe_3O_4/SiO_2 Core/Shell Nanocubes: Novel Coating Approach with Tunable Silica Thickness and Enhancement in Stability and Biocompatibility. Journal of Nanomedicine & Nanotechnology. 2014;05(06).
37. Issa B, Obaidat I, Albiss B, Haik Y. Magnetic Nanoparticles: Surface Effects and Properties Related to Biomedicine Applications. Int J Mol Sci. 2013;14(11):21266-21305.
38. Tian B, Wang T, Dong R, Bao S, Yang F, Zhang J. Core–shell structured γ-$Fe_2O_3@SiO_2@AgBr$:Ag composite with high magnetic separation efficiency and excellent visible light activity for acid orange 7 degradation. Applied Catalysis B: Environmental. 2014;147:22-28.